Composites Part B 241 (2022) 110011

Contents lists available at ScienceDirect

Composites Part B

journal homepage: www.elsevier.com/locate/compositesb

Nanoparticles distribution and agglomeration analysis in electrospun fiber based composites for desired mechanical performance of poly (3-hydroxybuty-rate-co-3-hydroxyvalerate (PHBV) scaffolds with hydroxyapatite (HA) and titanium dioxide (TiO_2) towards medical applications

Joanna E. Karbowniczek, Daniel P. Ura, Urszula Stachewicz *

Faculty of Metals Engineering and Industrial Computer Science, AGH University of Science and Technology, 30-059, Kraków, Poland

ARTICLE INFO

Keywords:
PHBV
Composite
Tensile tests
Stress-strain
Toughness
Nanoparticles
Distribution
Hydroxyapatite
Titanium dioxide

ABSTRACT

Scaffolds designed for tissue engineering must meet multiple criteria, including mechanical performance matching particular tissue properties. One of the strategies to improve electrospun scaffolds strength is the incorporation of ceramic nanoparticles. In this work, the effect of the addition of hydroxyapatite (HA) and titanium dioxide (TiO_2) nanoparticles on tensile strength, elongation and toughness of poly (3-hydroxybuty-rate-co-3-hydroxyvalerate (PHBV) based fibers was tested. Samples morphology along with chemical composition and particles distribution were characterized by scanning electron microscopy (SEM), energy dispersive X-ray spectroscopy (EDS) and Fourier transform infrared spectroscopy (FTIR). Mechanical properties of PHBV-based electrospun scaffolds were correlated with the nanoparticles' distributions examined via microscopy analysis to understand the failure mechanism of composite fibers. We observed a significant improvement of mechanical properties of composites containing HA nanoparticles compared with solely PHBV fibers. Notably, 3 times higher tensile strength and strain at failure, followed by 16 times improved toughness, was correlated with homogenous distribution of HA nanoparticles with an average area of aggregates reaching 0.11 μm^2. At the same time, two times larger TiO_2 aggregates were irregularly formed along PHBV fibers and caused deterioration of their mechanical properties. We showed the relevant strategy of particle distribution in fibers that are able to tailor mechanical properties by controlling the size and distribution of ceramic fillers in hybrid scaffolds.

1. Introduction

In tissue engineering, scaffolds are considered materials replacing extracellular matrix (ECM), providing mechanical and structural support for cell attachment, proliferation and tissue development. Proper 3D architecture and interconnected porosity are crucial to ensure nutrients and metabolites flow and allow cells migration and colonization of the entire scaffold. This supportive structures can additionally serve as carriers for drugs and other active compounds to induce desired cellular responses [1,2]. However, in guiding initial cell adhesion, formation of attachment points and further tissue development essential are scaffold's surface and bulk properties [3,4]. Tailoring material stiffness can improve durability, facilitate scaffold handling and plays a material-instructive role regulating cellular processes [5]. Actomyosin allows cell sense material rigidity and adopts cytoskeleton organization, focal adhesion sites formation and other biological processes related to successful in vitro tissue formation [6]. Importantly, cell-material interactions are dynamic and mutual. Physicochemical properties of the scaffold affect cell phenotype, differentiation and migration, but cells can also exert forces on the material [7,8]. Therefore, scaffold stiffness, rigidity and mechanical performance in cell culture conditions are essential parameters to be considered while designing tissue scaffolds.

Scaffolds should represent proper characteristic for each specific tissue creating a microenvironment that, together with growth factors, will lead to correct tissue regeneration. ECM of most tissues is based on collagen in the form of fibrous structures [9]. Similarly organized materials, serving as tissue scaffolds, could be produced by electrospinning [10], where a polymer solution is pushed through the nozzle with a

* Corresponding author.
E-mail address: ustachew@agh.edu.pl (U. Stachewicz).

https://doi.org/10.1016/j.compositesb.2022.110011
Received 13 March 2022; Received in revised form 22 April 2022; Accepted 31 May 2022
Available online 1 June 2022

controlled flow rate. The potential difference between nozzle and collector is a driving force for fibers formation. Droplet formed at the tip of the nozzle after overcoming surface tension under the influence of applied voltage is stretched to form fibers deposited at the collector [11,12]. Adjusting parameters during solution preparation, electrospinning settings, ambient conditions and postprocessing allow obtaining fibers and mats with desired morphology and properties [13]. Towards controlling of mechanical properties of scaffolds obtained by electrospinning, various strategies are exploited, including fibers orientation [14], diameter [15,16], porosity [17,18], core-shell structures [19], composites of two fiber types [20], or addition of ceramic particles [21–25].

Biodegradable poly (3-hydroxybuty-rate-co-3-hydroxyvalerate) (PHBV) belonging to polyhydroxyalkanoates (PHAs) synthetized by bacteria [26,27] can be processed via electrospinning and it has been studied for multiple biomedical applications: bone tissue regeneration [4,25,28], atopic skin treatment [27], antibacterial wound dressings [29,30], drug delivery systems [31]. PHBV is frequently combined with ceramic particles for biological purposes of improved in vitro cell growth (hydroxyapatite (HA), bioactive glass) or antibacterial activity (titanium dioxide (TiO_2), zinc oxide (ZnO)) [22,23,32,33]. An additional advantage of such hybrid structures is the increase of mechanical properties of relatively weak electrospun PHBV fibers [34]. Several strategies of preparing hybrid organic-inorganic PHBV-based scaffolds were tested: blend electrospinning [4], simultaneous electrospinning of polymer fibers and electrospraying of particles [35], soaking in simulated body fluid (SBF) [36]. The reinforcement effect of hard ceramic filler within polymer fibers is related to their concentration [21,25] as well as integration between two phases [35]. A small amount of up to several wt% of particles in polymer matrix improves the mechanical performance of electrospun scaffolds, which is often related to their homogenous distribution [37,38]. Presence of nanoparticles in the final composite depends on suspension stability before processing. Nanoparticles' dispersion is stabilized by electrostatic repulsion concerning the permanent charges on their surface. Additionally, in non-aqueous systems the colloidal stability is controlled by steric repulsion induced by adsorbed layers [39]. Zeta potential is a valuable indicator of colloidal stability of suspensions, with high absolute values conferring stability and low absolute values denoting the predominance of the attractive forces between the particles and the tendency to aggregate [40]. However, the exact distribution of the nanoparticles within fibers is rarely studied, and it is still challenging. Mainly transmission electron microscopy (TEM) on individual fibers is used, which is limited to the fiber diameter and may not represent an entire scaffold [38]. Importantly, TEM imaging of composite structures is applied to fibers with diameter below 1 μm to obtain the required transparency for electron beam [41,42]. For the higher fiber diameters different imaging methods should be employed. Other approach to visualize the distribution of ceramic additives within polymer network is energy dispersive X-ray (EDS) mapping, however for beam sensitive samples this method may introduce artifacts due to sample drift and deformation.

As the interest in hybrid biomaterials is growing a clear understanding of reinforcing composites strategies is required [43]. Incorporating nanoparticles in electrospun fibers often increase their stiffness [44,45], improving their biocompatibility and cell responses in tissue regeneration processes [8,46,47]. For this study, we selected the most used nanoparticles for bone regeneration scaffolds such as HA due to their proven bioactivity [25] and antibacterial TiO_2 [48]. Furthermore, the strength of composite fibers is strongly correlated with the concentration of nanoparticles, their sizes and distribution within the polymer matrix [32,35,49]. Therefore, we investigate the effect of HA and TiO_2 nanoparticles on the mechanical properties of electrospun PHBV fibers concerning their dispersion and aggregation in produced fibers. Using the advanced microscopy techniques based on secondary and backscatter electrons and energy dispersive X-ray spectroscopy, we verify the effect of nanoparticles type and their distribution in fibers on the strength, fracture, and toughness of the electrospun scaffolds in the random orientation of fibers for medical applications.

2. Materials and methods

2.1. Sample preparation - electrospinning

We electrospun four types of samples using PHBV (Helian Polymers, The Netherlands, M_w = 450,000 g mol^{-1}) solely and mixed with hydroxyapatite (HA) nanoparticles (particles size <200 nm, Sigma-Aldrich, UK) or titanium dioxide – TiO_2 nanoparticles (particles size <100 nm, Sigma-Aldrich, UK) or combination of both to prepare blend solutions. Different samples prepared for this study were named: PHBV, PHBV+HA, PHBV+TiO_2 and PHBV+HA+TiO_2. The primary solution of PHBV was prepared by dissolving 8 wt% in chloroform and dimethylformamide (DMF) v/v 9:1 by stirring on a heating plate (IKA, Germany) at a constant speed of 1000 rpm and temperature of 45 °C for 4 h. Solutions containing nanoparticles were additionally homogenized in an ultrasonic bath (Sonorex Bandelin, Germany) for 10 min prior to stirring and for 15 min before electrospinning. The concentration of nanoparticles in PHBV solutions was 1 wt% for HA and TiO_2 if one type of nanoparticles was added, and for the nanoparticles' mixture, it was 0.5 wt% of each nanoparticles type. Electrospinning was performed using a set-up with a climate control chamber (IME, The Netherlands), at RH = 40% and T = 25 °C. We kept all the same electrospinning parameters for all solutions: applied voltage of 17 kV, needle-collector distance of 20 cm, the flow rate of 0.1 ml min^{-1}. For mechanical testing, samples were deposited in random orientation for 4 min on specially designed paper frames with laser-cut rectangular (20 × 8 mm) holes mounted on the rotation drum (rotation speed of 10 rpm) [18].

2.2. Fibers' morphology and nanoparticles distribution analysis

The morphology of the obtained samples was investigated using scanning electron microscopy (SEM, Merlin, Zeiss, Germany) at 2 kV and 100 pA by secondary electrons (SE) detector. Samples were coated with 8 nm Au layer by a rotary pump sputter coater (Q150RS, Quorum Technologies, UK). The average fiber diameters ($D_{f\text{-}avg}$) were measured from 100 fibers from SEM images using the ImageJ software (v. 1.51j8, USA) and presented in the form of histograms. The presence of nanoparticles was confirmed by energy dispersive X-ray spectroscopy (EDS) using a detector (Brucker, Germany) and point analysis at 8 kV and 1000 pA. To study nanoparticles distribution as-received samples were imaged by SEM (Phenom ProX, Thermo Fisher Scientific, USA) equipped with backscattered electrons (BSE) detector at accelerating voltage of 10 kV. Next, SEM images were thresholded (intermodes, B&W) and binarized using ImageJ, which was also applied to determine the average particle area from 500 measurements using the particle analysis option.

To confirm the chemical composition of all electrospun samples, Attenuated Total Reflectance - Fourier Transform Infrared Spectroscopy (ATR-FTIR) was performed using Nicolet™ iS™ 5 FTIR Spectrometer (Thermo Fisher Scientific, USA) with the diamond crystal. During measurements, the spectra were 64 repeated over the wavenumber range 400–2000 cm^{-1}, with resolution 1 cm^{-1}.

2.3. Mechanical testing

Mechanical properties of scaffolds were verified using a tensile module equipped with a 1 N cell (B.1708.A, Kammrath& Weiss, Dortmund, Germany), at an extension rate 20 μm·s−1 at T = 24 °C and RH = 35%. The stress was calculated as a force measured by the tensile module to the initial cross-sectional area of the electrospun fiber scaffolds. Cross-sections of fibers deposited on paper frames were imaged by SEM; based on 5 measurements, the average thickness was calculated for each material. Toughness was determined by integrating each of the

stress-strain curves. The average maximum stress, toughness, strain at maximum stress and at failure were calculated from 3 tests for each material type. The morphology of uncoated samples after stretching was studied by SEM using a BSE detector, while details of fractured fibers were visualized by SE detector on coated samples.

3. Results and discussion

3.1. Morphology of fibers, nanoparticles distribution and chemical analysis

With all four types of PHBV based solutions, we produced randomly oriented smooth fibers, as shown in Fig. 1. The average fiber diameter ($D_{f\text{-}avg}$) for solely PHBV sample was 2.49 μm. Generally, the addition of ceramic nanoparticles resulted in increased fiber diameter. For PHBV+HA, the increase was up to 75%, the $D_{f\text{-}avg}$ reached 4.32 μm, for PHBV+TiO_2 the increase was 17%, and $D_{f\text{-}avg}$ was 2.92 μm, while for PHBV+HA+TiO_2 the increase was only 6% and $D_{f\text{-}avg}$ was 2.64 μm. PHBV fibers with the addition of ceramic nanoparticles have locally visible morphological changes compared to uniform PHBV fibers without them.

In Fig. 1, we can notice the nanoparticles agglomerations that are visible as beads-like structures, especially in the case of samples containing TiO_2 (Fig. 1 e, g). Notably, the presence of ceramic fillers within fibers structure differs between the samples, in both distribution and sizes of agglomerates, which is indicated by the measured nanoparticles area, see Fig. 2. HA nanoparticles are homogeneously distributed within the structure of the fibers forming small aggregates with an average size

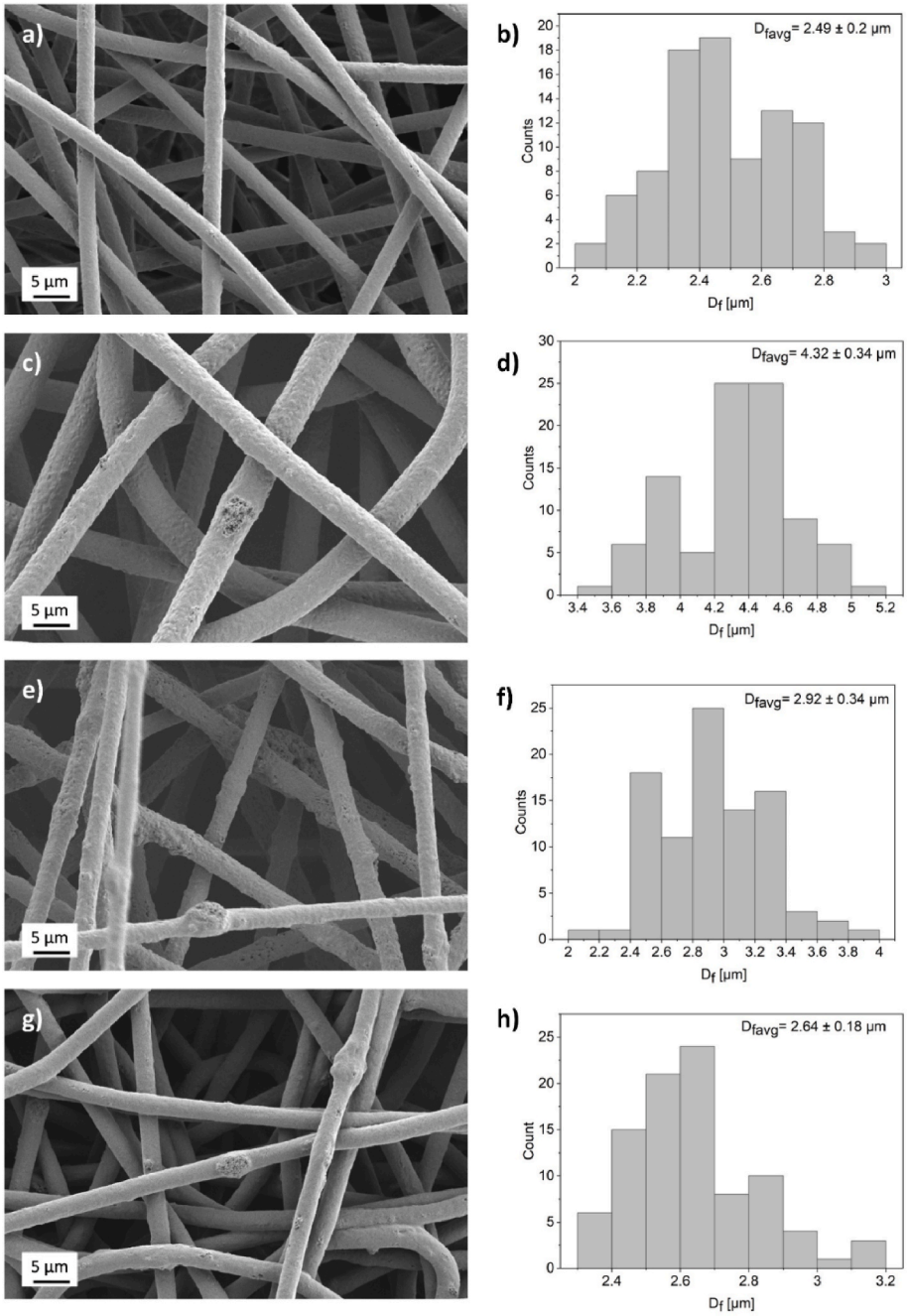

Fig. 1. SEM micrographs (SE) of electrospun fibers morphology and corresponding histograms presenting fiber diameters for samples: a, b) PHBV; c, d) PHBV+HA; e, f) PHBV+TiO_2; and g, h) PHBV+HA+TiO_2.

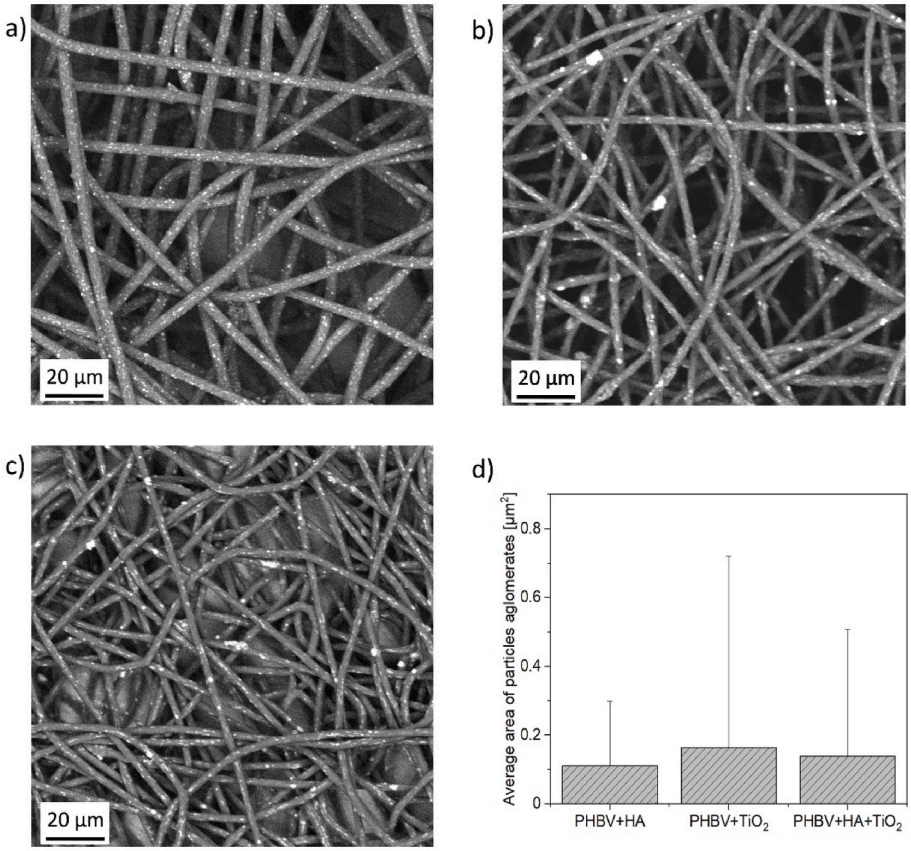

Fig. 2. SEM micrographs (BSE detector, uncoated samples) showing the distribution of particles within fibers: a) PHBV+HA; b) PHBV+TiO_2; c) PHBV+HA+TiO_2, and d) column chart showing the average area of nanoparticles aggregates in fibers.

area of 0.11 μm^2, mostly entirely covered by PHBV polymer. TiO_2 tend to form larger aggregates with average area of 0.22 μm^2. Nanoparticles distribution within fibers is less homogenous, in many cases, massive aggregates exceeding an area of 1 μm^2 are present at fibers surface, as we can see in Fig. 2 b. Samples containing both nanoparticles have an average size area of aggregates reaching 0.14 μm^2 and two models of large and small aggregates distributed within the fibers. Interestingly, in the PHBV+HA+TiO_2 sample, both nanoparticles did not mix; they were often present as separate agglomerates as shown by EDS analysis (Fig. 3 e-g).

By EDS we confirmed the presence of HA and TiO_2 in PHBV fibers using the point-by-point local analysis. At the same time, the FTIR measurements indicated the presence of the nanoparticles in the entire volume of all types of samples, see Fig. 4. FTIR analysis allowed us to identify characteristic peaks for all compounds in our electrospun samples. The predominant signal is from PHBV, with intense peak characteristic for a crystalline form of the polymer at around 1719 cm^{-1} associated with the C=O stretching [50]. Furthermore, various aliphatic C–H vibrational bands were observed in the range of 1227–1473 cm^{-1} and 825–980 cm^{-1}, while C–O vibration bands were recorded at 1181, 1129, and 1055 cm^{-1} [25,33]. Fibers with HA addition had distinct peaks at 569 and 602 cm^{-1} related to P–O stretching [25]. In the spectra of sample PHBV+TiO_2, we observed a broad absorption band between 500 and 800 cm^{-1} associated with the presence of TiO_2 particles and indicated as Ti–O and Ti–O–Ti bridging stretching [51]. For sample PHBV+HA+TiO_2 containing both types of particles, but in lower quantities, as the particles in the PHBV solution had to be adjusted, the peaks and regions characteristic for additives are also present at the lower intensity level.

3.2. Mechanical properties

Tensile tests of electrospun PHBV scaffolds showed a relatively low mechanical performance with the tensile strength of 82 kPA, see all the stress-strain characteristics in Fig. 5. PHB polymers are brittle, and only by copolymerizing the PHB homopolymer with the HV monomer, they gain elasticity [52]. The weak mechanical performance of PHBV fibers was even 50% reduced to the average stress of 41 kPA when TiO_2 nanoparticles were added, see Table 1. The highest tensile stress was obtained in the samples with the HA addition, reaching 215 kPa for PHBV+HA and 244 kPA for PHBV+HA+TiO_2.

PHBV fibers break easily during the tensile tests at many locations along the individual fiber. In Fig. 6 a, b, the fractured PHBV fibers show a clear cross-section with almost sharp borders. The cracks and notches are visible in many places on the fibers indicating a brittle characteristic of PHBV. The addition of ceramic nanoparticles in all configurations improved the ductility of scaffolds as the strain at failure was 3 times higher for PHBV+HA+TiO_2 and about 5 times higher for PHBV+HA and PHBV+TiO_2 samples. Similarly, Kim et al. [17] observed the transition of PMMA fibers from brittle structures to ductile by a well-controlled electrospinning process and the formation of nanoporous morphology on fiber surface.

The homogenous distribution of HA nanoparticles increased the diameter of PHBV fibers, followed by the improved mechanical performance, by the significantly higher maximum tensile strength and elongation, see Fig. 5. Next, in Fig. 6 c, we show a sausage-like structure with the characteristic thickening of PHBV+HA fibers at the places where the breakage starts. It causes fibers' elongation at the place where the crack appears in the form of stretch marks, see Fig. 6 d. Here, the small aggregates of HA nanoparticles acted as barriers in crack propagation. The reinforcement of electrospun fibers has been studied previously,

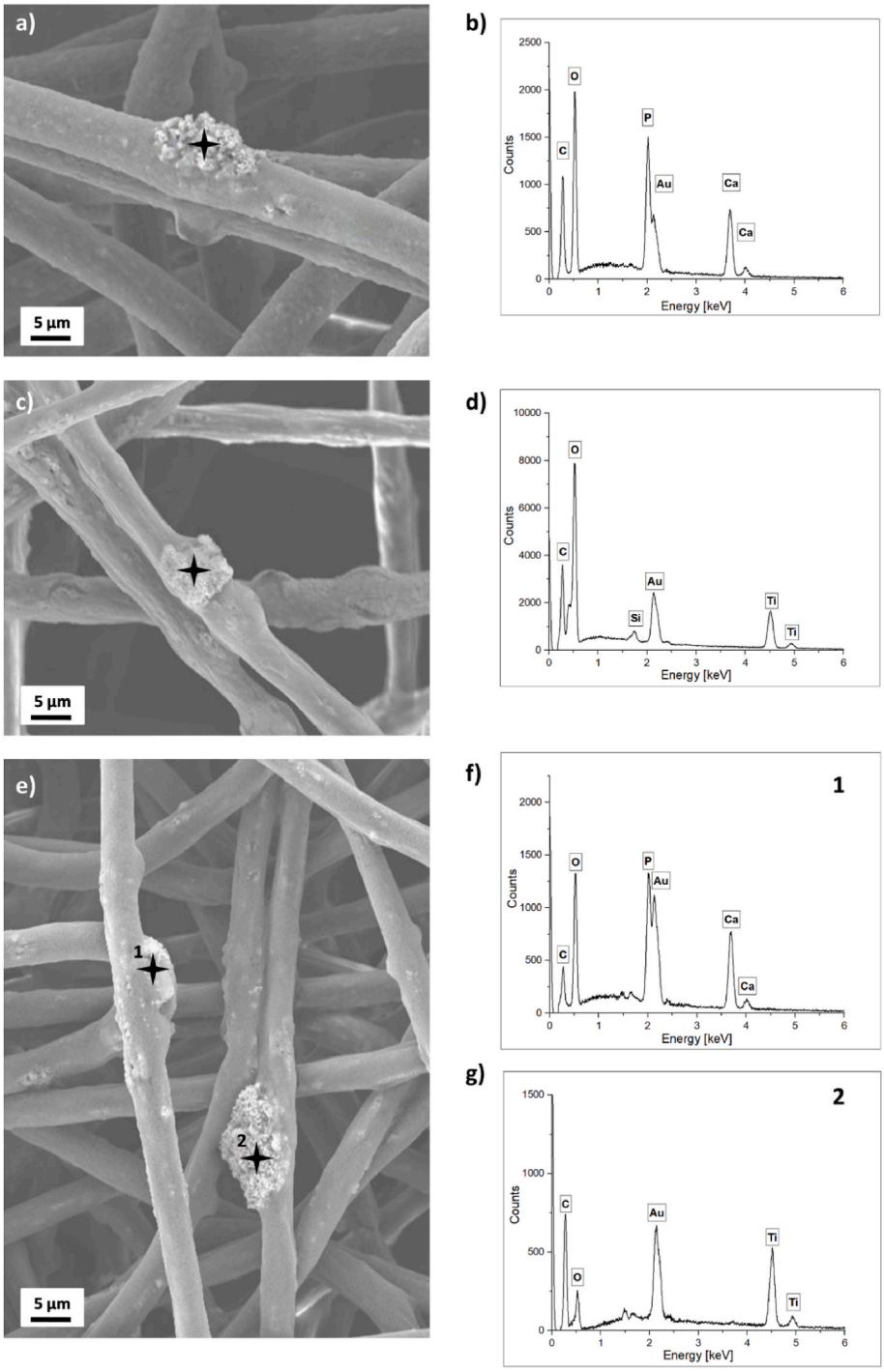

Fig. 3. SEM micrographs (SE) with marked points of chemical elements analysis and corresponding EDS spectrum: a, b) PHBV+HA; c, d) PHBV+TiO_2; e, f, g) PHBV+HA+TiO_2.

indicating that nanoparticles in low concentrations improve mechanical properties. At the same time, agglomerations can weaken their mechanical performance by creating defect-like structures in fibers [21]. Another critical characteristic is nanoparticles distribution and the interface between nanoparticles and polymer matrix that can provide appropriate load transfer during tensile stretching. In blend electrospinning, when polymer solution contains a high particle concentration, agglomerations often occur. These agglomerations depend on the dispersion steps used in the preparation methods prior to fiber production. Evidently, the dispersion of the nanoparticles in the polymer solution affects their distribution in the produced fibers. The obtained clusters of the nanoparticles within fiber are often local stress concentration regions leading to the faster breakage of fibers, which is deteriorating mechanical properties of electrospun scaffolds [21,25]. The strength of the binding between particles and polymer fibers also affects the mechanical performance of the composite. In the case of blend electrospinning particles are mainly surrounded by polymer and provide improvement in load transfer [25]. In contrast, sputtered particles are weakly integrated with fibers, often only decorating their surface and can contribute to the decreased mechanical strength of the scaffold [35]. The other observed toughening mechanisms of electrospun fibers are multiple necking and crazing visible on PHBV+HA fibers (Fig. 6 c),

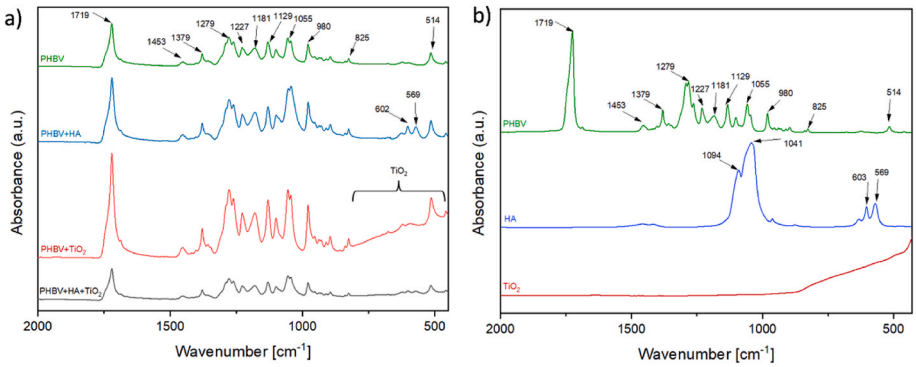

Fig. 4. The ATR–FTIR spectra of a) electrospun samples: PHBV, PHBV+HA, PHBV+TiO_2, PHBV+HA+TiO_2, b) powders (PHBV, HA, TiO_2) used to prepare solutions for electrospinning.

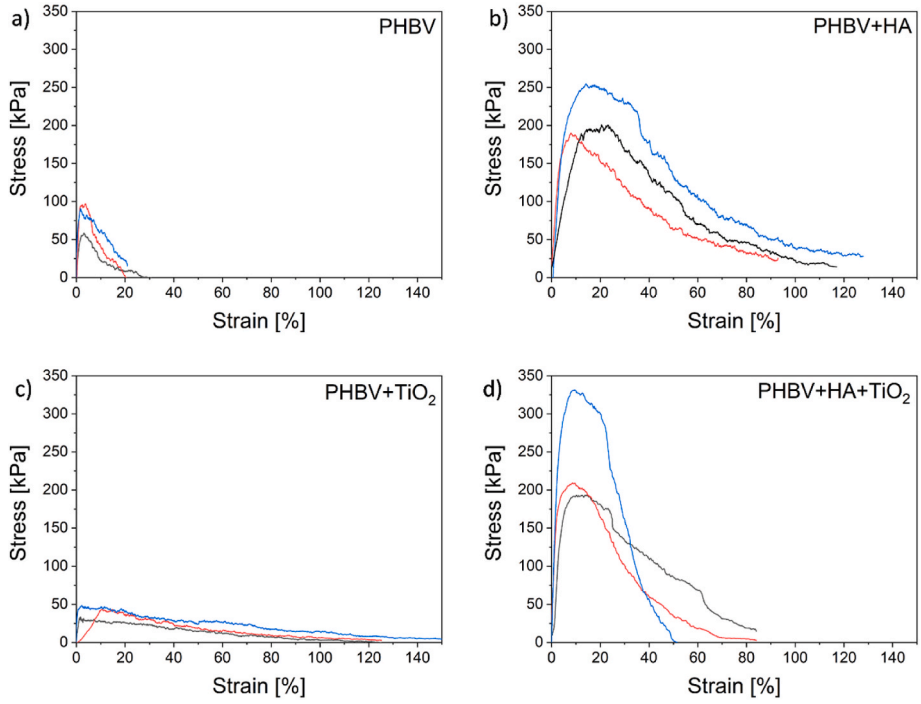

Fig. 5. Stress-strain curves of electrospun scaffolds: a) PHBV; b) PHBV+HA; c) PHBV+TiO_2; and d) PHBV+HA+TiO_2.

Table 1
Mechanical properties of electrospun scaffolds calculated from all the measurements.

Sample	Tensile strength σ [kPa]	Strain at max stress ε_{max} [%]	Strain at failure ε_f [%]	Toughness W [MJm^{-3}]
PHBV	82 ± 17	3.0 ± 0.8	23 ± 3	0.75 ± 0.15
PHBV+HA	215 ± 28	14.2 ± 5.1	112 ± 15	12.17 ± 19.50
PHBV+TiO_2	41 ± 6	4.7 ± 3.8	127 ± 3	1.39 ± 0.25
PHBV+HA+TiO_2	244 ± 62	11.3 ± 2.6	73 ± 16	8.58 ± 0.62

contributing to energy absorption [53]. Interestingly, PHBV+TiO_2 scaffolds were even weaker than solely PHBV polymer ones. The fiber breakage often happened at large aggregates of TiO_2 nanoparticles, as observed on the fibers shown in Fig. 6 e, f. The accumulation of TiO_2 nanoparticles significantly decreased tensile strength of PHBV+TiO_2 scaffolds. Here, the nanoparticle clusters worked as structural defects, as a similar effect was observed for fibers with beads [16]. For the samples with both types of nanoparticles (PHBV+HA+TiO_2) the tensile strength was the highest. Here, we noticed several crack propagation mechanisms with multiple necking and breaking points at high particles concentration regions (Fig. 6 g, h). These combinations of fibers deformation, allowed to increase fracture resistance for hybrid PHBV scaffolds. Among all tested samples the highest toughness was measured for PHBV+HA, 12.17 MJm^{-3}, giving the 16 times increase in comparison to PHBV sample as indicated in Table 1.

Indeed, the mechanical properties of polymer composites depend on the polydispersity of the reinforcement fractions [54]. However, in the electrospun membranes, the interactions between fibers in random orientation [55] and the adhesion between them [56] increase their fracture toughness and cause stress delocalization in the network. The failure mechanism depends on the strength of the individual fibers [57], their size [58], the parameters used in electrospinning [18,59] and the polymer solution composition. The fibers interaction, especially between fibers with the agglomerated nanoparticles, also created the interlocking system, resulting in the network's damage [37]. In many natural and bioinspired polymeric materials, the mechanical properties are the synergetic effect of stress dissipation by including stiffer reinforcement components in the composites [60,61].

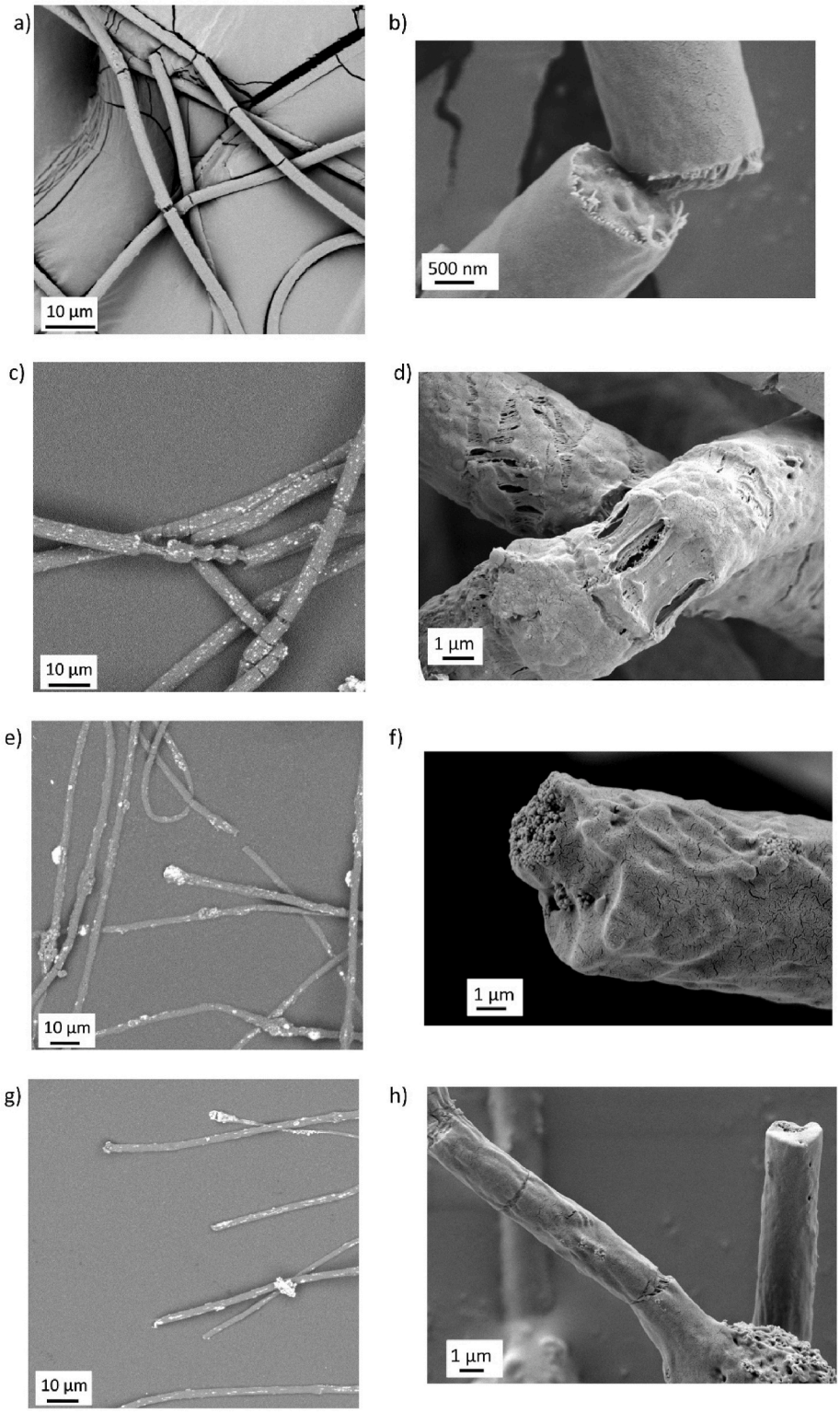

Fig. 6. SEM micrographs of fractured electrospun fibers after mechanical testing: a) PHBV (BSD, coated); b) PHBV (SE, coated); c) PHBV+HA (BSE, uncoated); d) PHBV+HA (SE, coated); e) PHBV+TiO_2 (BSE, uncoated); f) PHBV+TiO_2 (SE, coated); g) PHBV+HA+TiO_2 (BSE, uncoated); h) PHBV+HA+TiO_2 (SE, coated).

Considering the differences in HA and TiO_2 nanoparticles distribution, even the polymer-ceramic blends for electrospinning and the production were similar. Interestingly, the zeta potential of the nanoparticles varies. Zeta potential in pH 7.4 for HA nanoparticles (same as solvents mixture used in this work) is approximately −20 mV [40]. The relatively high negative potential for HA nanoparticles suggests a low tendency to their aggregation. In contrast, TiO_2 nanoparticles (anatase and rutile mixture, like in our study) are nearly neutral for the same pH. Additionally, the relatively high polydispersity index value contributes to increased nanoparticles aggregation [62]. This property indicates that the dispersion of nanoparticles depends not only on the preparation method of composites and the sizes of nanoparticles but their surface properties, such as zeta potential.

The accumulation of nanoparticles reduces the interfacial

interactions with the polymer matrix, thus weakening the interfacial strength between them and decreasing the load transfer abilities of produced composite fibers [21]. In fibrous composite, the interfaces are essential to enhance mechanical performance [63]. The internal structure of polymer fibers, including core-shell structures, can be controlled by the polymer and solvent selection in electrospinning [64]. The core-shell systems are also used to reinforce individual fibers [19] and all membranes [65]. The versatility of electrospinning gives a lot of possibilities to create hybrid fibers often used as scaffolds for tissue regeneration, which underlines the importance of understanding the structure-properties and structure-function relationships for designing biomaterials.

4. Conclusions

This work showed the importance of ceramic nanoparticles distribution and aggregate size effect on the mechanical properties of PHBV-based electrospun scaffolds. The rigid structure obtained in the PHBV+HA sample due to small aggregates of nanoparticles homogeneously dispersed in the polymer fibers improved fracture toughness 16 times compared to unmodified PHBV fibers. While the addition of TiO_2 in our system caused the deterioration of tensile strength by large particles aggregated working as local defect sides weakening fibers. Various advanced imaging techniques were applied to analyses the nanoparticles distribution in electrospun scaffolds and to understand the reinforcement mechanism in electrospun fibers, which has many fundamental implications in the tissue engineering. Importantly, we showed that designing hybrid fibrous scaffolds with the primary goal of biological activity of the structure resulting from ceramic filler we should consider their effect on mechanical properties.

Author statement

J. E. K. Methodology, Visualization, Investigation, Conceptualization, Resources, Writing- Original draft preparation, Writing - Review & Editing, Project administration, Funding acquisition.

D. P. U. Methodology, Visualization, Investigation, Writing - Review & Editing.

U·S.: Supervision, Methodology, Conceptualization, Resources, Writing- Original draft preparation, Writing - Review & Editing, Project administration, Funding acquisition.

Declaration of competing interest

The authors declare that they have no known competing financial interests or personal relationships that could have appeared to influence the work reported in this paper.

Acknowledgment

The study was financially supported by the grant PRELUDIUM 15, No2018/29/N/ST8/02032 financed by National Science Center in Poland. The mechanical testing and FTIR analysis were supported by the BioCom4SavEn project funded by the European Research Council under the European Union's Horizon 2020 Framework Programme for Research and Innovation (ERC grant agreement no. 948840).

References

[1] Arun A, Malrautu P, Laha A, Ramakrishna S. Gelatin nanofibers in drug delivery systems and tissue engineering. Eng Sci 2021;16:71–81. https://doi.org/10.30919/es8d527.

[2] Deng L, Zhang H. Recent advances in probiotics encapsulation by electrospinning. ES Food Agrofor 2020;3–12. https://doi.org/10.30919/esfaf1120.

[3] Abdal-hay A, Raveendran NT, Fournier B, Ivanovski S. Fabrication of biocompatible and bioabsorbable polycaprolactone/magnesium hydroxide 3D printed scaffolds: degradation and in vitro osteoblasts interactions. Compos B Eng 2020;197. https://doi.org/10.1016/j.compositesb.2020.108158.

[4] Karbowniczek JE, Kaniuk Ł, Berniak K, Gruszczyński A, Stachewicz U. Enhanced cells anchoring to electrospun hybrid scaffolds with PHBV and HA particles for bone tissue regeneration. Front Bioeng Biotechnol 2021;9:1–13. https://doi.org/10.3389/fbioe.2021.632029.

[5] Xing F, Li L, Zhou C, Long C, Wu L, Lei H, et al. Regulation and directing stem cell fate by tissue engineering functional microenvironments: scaffold physical and chemical cues. Stem Cell Int 2019:1–16. https://doi.org/10.1155/2019/2180925. 2019.

[6] Doss BL, Pan M, Gupta M, Grenci G, Mège RM, Lim CT, et al. Cell response to substrate rigidity is regulated by active and passive cytoskeletal stress. Proc Natl Acad Sci U S A 2020;117:12817–25. https://doi.org/10.1073/pnas.1917555117.

[7] Meehan S, Nain AS. Role of suspended fiber structural stiffness and curvature on single-cell migration, nucleus shape, and focal-adhesion-cluster length. Biophys J 2014;107:2604–11. https://doi.org/10.1016/j.bpj.2014.09.045.

[8] Yi B, Xu Q, Liu W. An overview of substrate stiffness guided cellular response and its applications in tissue regeneration. Bioact Mater 2022;15:82–102. https://doi.org/10.1016/j.bioactmat.2021.12.005.

[9] Patterson J, Martino MM, Hubbell JA. Biomimetic materials in tissue engineering. Mater Today 2010;13:14–22. https://doi.org/10.1016/S1369-7021(10)70013-4.

[10] Agarwal S, Wendorff JH, Greiner A. Use of electrospinning technique for biomedical applications. Polymer 2008;49:5603–21. https://doi.org/10.1016/j.polymer.2008.09.014.

[11] Theron SA, Zussman E, Yarin AL. Experimental investigation of the governing parameters in the electrospinning of polymer solutions. Polymer 2004;45. https://doi.org/10.1016/j.polymer.2004.01.024. 2017–30.

[12] Hohman MM, Shin M, Rutledge G, Brenner MP. Electrospinning and electrically forced jets. I. Stability theory. Phys Fluids 2001;13:2201–20. https://doi.org/10.1063/1.1383791.

[13] Rutledge GC, Fridrikh SV. Formation of fibers by electrospinning. Adv Drug Deliv Rev 2007;59:1384–91. https://doi.org/10.1016/j.addr.2007.04.020.

[14] Maciel MM, Ribeiro S, Ribeiro C, Francesko A, Maceiras A, Vilas JL, et al. Relation between fiber orientation and mechanical properties of nano-engineered poly (vinylidene fluoride) electrospun composite fiber mats. Compos B Eng 2018;139:146–54. https://doi.org/10.1016/j.compositesb.2017.11.065.

[15] Lü LX, Wang YY, Mao X, Xiao ZD, Huang NP. The effects of PHBV electrospun fibers with different diameters and orientations on growth behavior of bone-marrow-derived mesenchymal stem cells. Biomed Mater 2012;7. https://doi.org/10.1088/1748-6041/7/1/015002.

[16] Huan S, Liu G, Han G, Cheng W, Fu Z, Wu Q, et al. Effect of experimental parameters on morphological, mechanical and hydrophobic properties of electrospun polystyrene fibers. Materials 2015;8:2718–34. https://doi.org/10.3390/ma8052718.

[17] Kim GM, Lach R, Michler GH, Chang YW. The mechanical deformation process of electrospun polymer nanocomposite fibers. Macromol Rapid Commun 2005;26:728–33. https://doi.org/10.1002/marc.200500023.

[18] Szewczyk PK, Ura DP, Stachewicz U. Humidity controlled mechanical properties of electrospun polyvinylidene fluoride (PVDF) fibers. Fibers 2020;8:1–9. https://doi.org/10.3390/fib8100065.

[19] Ura DP, Berniak K, Stachewicz U. Critical length reinforcement in core-shell electrospun fibers using composite strategies. Compos Sci Technol 2021;211:108867. https://doi.org/10.1016/j.compscitech.2021.108867.

[20] Knapczyk-Korczak J, Ura DP, Gajek M, Marzec MM, Berent K, Bernasik A, et al. Fiber-based composite meshes with controlled mechanical and wetting properties for water harvesting. ACS Appl Mater Interfaces 2020;12:1665–76. https://doi.org/10.1021/acsami.9b19839.

[21] Doustgani A, Vasheghani-Farahani E, Soleimani M, Hashemi-Najafabadi S. Optimizing the mechanical properties of electrospun polycaprolactone and nanohydroxyapatite composite nanofibers. Compos B Eng 2012;43:1830–6. https://doi.org/10.1016/j.compositesb.2012.01.051.

[22] Braga NF, Vital DA, Guerrini LM, Lemes AP, Formaggio DMD, Tada DB, et al. PHBV-TiO2 mats prepared by electrospinning technique: physico-chemical properties and cytocompatibility. Biopolymers 2018;109:1–12. https://doi.org/10.1002/bip.23120.

[23] Naphade R, Jog J. Electrospinning of PHBV/ZnO membranes: structure and properties. Fibers Polym 2012;13:692–7. https://doi.org/10.1007/s12221-012-0692-9.

[24] Ivanoska-Dacikj A, Bogoeva-Gaceva G, Krumme A, Tarasova E, Scalera C, Stojkovski V, et al. Biodegradable polyurethane/graphene oxide scaffolds for soft tissue engineering : in vivo behavior assessment. Int J Polym Mater Polym Biomater 2020;69:1–11. https://doi.org/10.1080/00914037.2019.1655754.

[25] Kouhi M, Prabhakaran MP, Shamanian M, Fathi M, Morshed M, Ramakrishna S. Electrospun PHBV nanofibers containing HA and bredigite nanoparticles: fabrication, characterization and evaluation of mechanical properties and bioactivity. Compos Sci Technol 2015;121:115–22. https://doi.org/10.1016/j.compscitech.2015.11.006.

[26] Rehm BHA. Bacterial polymers: biosynthesis, modifications and applications. Nat Rev Microbiol 2010;8:578–92. https://doi.org/10.1038/nrmicro2354.

[27] Kaniuk Ł, Stachewicz U. Development and advantages of biodegradable PHA polymers based on electrospun PHBV fibers for tissue engineering and other biomedical applications. ACS Biomater Sci Eng 2021;7:5339–62. https://doi.org/10.1021/acsbiomaterials.1c00757.

[28] Paşcu EI, Stokes J, McGuinness GB. Electrospun composites of PHBV, silk fibroin and nano-hydroxyapatite for bone tissue engineering. Mater Sci Eng C 2013;33:4905–16. https://doi.org/10.1016/j.msec.2013.08.012.

[29] Augustine R, Hasan A, Patan NK, Dalvi YB, Varghese R, Antony A, et al. Cerium oxide nanoparticle incorporated electrospun poly(3-hydroxybutyrate-co-3-

hydroxyvalerate) membranes for diabetic wound healing applications. ACS Biomater Sci Eng 2020;6:58–70. https://doi.org/10.1021/acsbiomaterials.8b01352.
[30] Abdalkarim SYH, Yu HY, Wang D, Yao J. Electrospun poly(3-hydroxybutyrate-co-3-hydroxy-valerate)/cellulose reinforced nanofibrous membranes with ZnO nanocrystals for antibacterial wound dressings. Cellulose 2017;24:2925–38. https://doi.org/10.1007/s10570-017-1303-0.
[31] Liu Y, Chen X, Yu DG, Liu H, Liu Y, Liu P. Electrospun PVP-core/PHBV-shell fibers to eliminate tailing off for an improved sustained release of curcumin. Mol Pharm 2021;18:4170–8. https://doi.org/10.1021/acs.molpharmaceut.1c00559.
[32] Peranidze K, Safronova TV, Kildeeva NR. Fibrous polymer-based composites obtained by electrospinning for bone tissue engineering. Polymers 2022;14:1–19. https://doi.org/10.3390/polym14010096.
[33] Kouhi M, Fathi M, Prabhakaran MP, Shamanian M, Ramakrishna S. Enhanced proliferation and mineralization of human fetal osteoblast cells on PHBV-bredigite nanofibrous scaffolds. Mater Today Proc 2018;5:15702–9. https://doi.org/10.1016/j.matpr.2018.04.181.
[34] Kaniuk Ł, Podborska A, Stachewicz U. Enhanced mechanical performance and wettability of PHBV fiber blends with evening primrose oil for skin patches improving hydration. J Mater Chem B 2022;10:1763–74. https://doi.org/10.1039/d1tb02805g.
[35] Ramier J, Bouderlique T, Stoilova O, Manolova N, Rashkov I, Langlois V, et al. Biocomposite scaffolds based on electrospun poly (3-hydroxybutyrate) nanofi bers and electrosprayed hydroxyapatite nanoparticles for bone tissue engineering applications. Mater Sci Eng C 2014;38:161–9. https://doi.org/10.1016/j.msec.2014.01.046.
[36] Ito Y, Hasuda H, Kamitakahara M, Ohtsuki C, Tanihara M, Kang IK, et al. A composite of hydroxyapatite with electrospun biodegradable nanofibers as a tissue engineering material. J Biosci Bioeng 2005;100:43–9. https://doi.org/10.1263/jbb.100.43.
[37] Rashid TU, Gorga RE, Krause WE. Mechanical properties of electrospun fibers—a critical review. Adv Eng Mater 2021;23:1–26. https://doi.org/10.1002/adem.202100153.
[38] Cai N, Li C, Luo X, Xue Y, Shen L, Yu F. A strategy for improving mechanical properties of composite nanofibers through surface functionalization of fillers with hyperbranched polyglycerol. J Mater Sci 2016;51:797–808. https://doi.org/10.1007/s10853-015-9403-4.
[39] Nguyen VS, Rouxel D, Vincent B. Dispersion of nanoparticles: from organic solvents to polymer solutions. Ultrason Sonochem 2014;21:149–53. https://doi.org/10.1016/j.ultsonch.2013.07.015.
[40] Wu F, Lin DDW, Chang JH, Fischbach C, Estroff LA, Gourdon D. Effect of the materials properties of hydroxyapatite nanoparticles on fibronectin deposition and conformation. Cryst Growth Des 2015;15:2452–60. https://doi.org/10.1021/acs.cgd.5b00231.
[41] Zhang Z, Zhao Y, Li Z, Zhang L, Liu Z, Long Z, et al. Synthesis of carbon/SiO2 core-sheath nanofibers with Co-Fe nanoparticles embedded in via electrospinning for high-performance microwave absorption. Adv Compos Hybrid Mater 2022;5:513–24. https://doi.org/10.1007/s42114-021-00350-w.
[42] Ziyadi H, Baghali M, Bagherianfar M, Mehrali F, Faridi-Majidi R. An investigation of factors affecting the electrospinning of poly (vinyl alcohol)/kefiran composite nanofibers. Adv Compos Hybrid Mater 2021;4:768–79. https://doi.org/10.1007/s42114-021-00230-3.
[43] Krysiak ZJ, Gawlik MZ, Knapczyk-Korczak J, Kaniuk L, Stachewicz U. Hierarchical composite meshes of electrospun PS microfibers with PA6 nanofibers for regenerative medicine. Materials 2020;13:11–3. https://doi.org/10.3390/MA13081974.
[44] Liverani L, Lacina J, Roether JA, Boccardi E, Killian MS, Schmuki P, et al. Incorporation of bioactive glass nanoparticles in electrospun PCL/chitosan fibers by using benign solvents. Bioact Mater 2018;3:55–63. https://doi.org/10.1016/j.bioactmat.2017.05.003.
[45] Niemczyk-Soczynska B, Zaszczyńska A, Zabielski K, Sajkiewicz P. Hydrogel, electrospun and composite materials for bone/cartilage and neural tissue engineering. Materials 2021;14:1–23. https://doi.org/10.3390/ma14226899.
[46] Ferraris S, Spriano S, Scalia AC, Cochis A, Rimondini L, Cruz-Maya I, et al. Topographical and biomechanical guidance of electrospun fibers for biomedical applications. Polymers 2020;12:1–32. https://doi.org/10.3390/polym12122896.
[47] Cai S, Wu C, Yang W, Liang W, Yu H, Liu L. Recent advance in surface modification for regulating cell adhesion and behaviors. Nanotechnol Rev 2020;9:971–89. https://doi.org/10.1515/ntrev-2020-0076.
[48] Cazan C, Enesca A, Andronic L. Synergic effect of tio 2 filler on the mechanical properties of polymer nanocomposites. Polymers 2021;13:1–24. https://doi.org/10.3390/polym13122017.
[49] Pryadko A, Surmeneva MA, Surmenev RA. Review of hybrid materials based on polyhydroxyalkanoates for tissue engineering applications. Polymers 2021;13. https://doi.org/10.3390/polym13111738.
[50] Brunetti L, Degli Esposti M, Morselli D, Boccaccini AR, Fabbri P, Liverani L. Poly (hydroxyalkanoate)s meet benign solvents for electrospinning. Mater Lett 2020;278:128389. https://doi.org/10.1016/j.matlet.2020.128389.
[51] Praveen P, Viruthagiri G, Mugundan S, Shanmugam N. Structural, optical and morphological analyses of pristine titanium di-oxide nanoparticles - synthesized via sol-gel route. Spectrochim Acta Part A Mol Biomol Spectrosc 2014;117:622–9. https://doi.org/10.1016/j.saa.2013.09.037.
[52] Pan P, Inoue Y. Polymorphism and isomorphism in biodegradable polyesters. Prog Polym Sci 2009;34:605–40. https://doi.org/10.1016/j.progpolymsci.2009.01.003.
[53] Tan CJ, Andriyana A, Ang BC, Wong D. Mechanical deformation and fracture mechanisms of polymeric fibres from the perspective of fractography – a review. Eur Polym J 2020;137:109924. https://doi.org/10.1016/j.eurpolymj.2020.109924.
[54] Engelberg I, Kohn J. Physico-mechanical properties of degradable polymers used in medical applications: a comparative study. Biomaterials 1991;12:292–304. https://doi.org/10.1016/0142-9612(91)90037-B.
[55] Stachewicz U, Peker I, Tu W, Barber AH. Stress delocalization in crack tolerant electrospun nanofiber networks. ACS Appl Mater Interfaces 2011;3. https://doi.org/10.1021/am2002444. 1991–6.
[56] Stachewicz U, Hang F, Barber AH. Adhesion anisotropy between contacting electrospun fibers. Langmuir 2014;30:6819–25. https://doi.org/10.1021/la5004337.
[57] Mannarino MM, Rutledge GC. Mechanical and tribological properties of electrospun PA 6(3)T fiber mats. Polymer 2012;53:3017–25. https://doi.org/10.1016/j.polymer.2012.04.039.
[58] Arinstein A, Burman M, Gendelman O, Zussman E. Effect of supramolecular structure on polymer nanofibre elasticity. Nat Nanotechnol 2007;2:59–62. https://doi.org/10.1038/nnano.2006.172.
[59] Stachewicz U, Bailey RJ, Wang W, Barber AH. Size dependent mechanical properties of electrospun polymer fibers from a composite structure. Polymer 2012;53:5132–7. https://doi.org/10.1016/j.polymer.2012.08.064.
[60] Metwally S, Stachewicz U. Teeth resorption at cement - enamel junction (CEJ) - microscopy analysis. Micron 2020;137:102913. https://doi.org/10.1016/j.micron.2020.102913.
[61] Stachewicz U. Microstructure study of fractured polar bear hair for toughening, strengthening, stiffening designs: via energy dissipation and crack deflection mechanisms in materials. Mol Syst Des Eng 2021;6:997–1002. https://doi.org/10.1039/d1me00066g.
[62] Korábková E, Kašpárková V, Jasenská D, Moricová D, Daďová E, Truong TH, et al. Behaviour of titanium dioxide particles in artificial body fluids and human blood plasma. Int J Mol Sci 2021;22. https://doi.org/10.3390/ijms221910614.
[63] Stachewicz U, Modaresifar F, Bailey RJ, Peijs T, Barber AH. Manufacture of void-free electrospun polymer nanofiber composites with optimized mechanical properties. ACS Appl Mater Interfaces 2012;4:2577–82. https://doi.org/10.1021/am300235r.
[64] Camposeo A, Greenfeld I, Tantussi F, Pagliara S, Moffa M, Fuso F, et al. Local mechanical properties of electrospun fibers correlate to their internal nanostructure. Nano Lett 2013;13:5056–62. https://doi.org/10.1021/nl4033439.
[65] Yang X, Wang J, Guo H, Liu L, Xu W, Duan G. Structural design toward functional materials by electrospinning: a review. E-Polymers 2020;20:682–712. https://doi.org/10.1515/epoly-2020-0068.